Nuclear Engineering and Technology 50 (2018) 35–42

Contents lists available at ScienceDirect

Nuclear Engineering and Technology

journal homepage: www.elsevier.com/locate/net

Original Article

Neutronics analysis of TRIGA Mark II research reactor

Haseebur Rehman [a], Siraj-ul-Islam Ahmad [b, *]

[a] Department of Nuclear Engineering, PIEAS, Nilore, Islamabad, Pakistan
[b] Research in Modeling and Simulation (RIMS) Group, Department of Physics, CIIT, Park Road, Islamabad, Pakistan

ARTICLE INFO

Article history:
Received 9 March 2017
Received in revised form
27 September 2017
Accepted 16 November 2017
Available online 8 December 2017

Keywords:
Control rod worth
Criticality calculations
ENDF/B-VI
ENDF/B-VII
JEF-2.2
JEFF-3.1
JENDL-3.2
Program for Reactor In-core Analysis using Diffusion Equation
TRIGA reactor
Winfrith Improved Multi-group Scheme-D/4

ABSTRACT

This article presents clean core criticality calculations and control rod worth calculations for TRIGA (Training, Research, Isotope production-General Atomics) Mark II research reactor benchmark cores using Winfrith Improved Multi-group Scheme-D/4 (WIMS-D/4) and Program for Reactor In-core Analysis using Diffusion Equation (PRIDE) codes. Cores 133 and 134 were analyzed in 2-D (r, θ) and 3-D (r, θ, z), using WIMS-D/4 and PRIDE codes. Moreover, the influence of cross-section data was also studied using various libraries based on Evaluated Nuclear Data File (ENDF/B-VI.8 and VII.0), Joint Evaluated Fission and Fusion File (JEFF-3.1), Japanese Evaluated Nuclear Data Library (JENDL-3.2), and Joint Evaluated File (JEF-2.2) nuclear data. The simulation results showed that the multiplication factor calculated for all these data libraries is within 1% of the experimental results. The reactivity worth of the control rods of core 134 was also calculated with different homogenization approaches. A comparison was made with experimental and reported Monte Carlo results, and it was found that, using proper homogenization of absorber regions and surrounding fuel regions, the results obtained with PRIDE code are significantly improved.

1. Introduction

The specifications of TRIGA Mark-II core 133 is among the standard benchmark cores for criticality safety calculations and has also been included in the International Handbook of Evaluated Criticality Safety Benchmark Experiments. Core 134 is a rearrangement of core 133 with some additional fuel elements to increase the excess reactivity. Various steady state and transient benchmark experiments were performed at TRIGA Mark II, Jožef Stefan Institute, Ljubljana [22], using both the cores to measure the excess reactivity, control rod (CR) worth, and fuel element reactivity worth [18] šč. The availability of experimental results for both the cores is also a key factor for the selection of these cores for analysis. This article presents the use of cylindrical (r, θ) and (r, θ, z) modeling of the Program for Reactor In-core Analysis using Diffusion Equation (PRIDE) code for the analysis of clean core and CR worth calculations.

To perform whole core analysis with diffusion theory codes, the geometry of the core and group constants for various homogenized regions of the core, along with fission spectrum data, are needed. In this study, group constants were generated using well-known 1-D transport theory code WIMS-D/4 and were used for the whole core calculations with PRIDE code. The procedure for defining various homogenized regions of the core to model in PRIDE is illustrated later in this article.

The code WIMS-D/4 uses its own processed cross-section data library. Several updated WIMSD libraries based on recently released cross-section data were made available by International Atomic Energy Agency (IAEA). These include ENDF/B-VI.8 [16], ENDF/B-VII.0 [8], JENDL-3.2 [20], JEF-2.2 (IAEA, 1993), and JEFF-3.1 [13]. In addition to WIMSD libraries based on these individual cross-section data sets, the WIMSD-IAEA library (which we refer to here as the IAEA library) was also released; it was developed by taking suitable cross-section data from different cross-section data sets [2,4]. The core calculations were also performed based on different WIMSD libraries, and intercomparison of the results is presented.

Control rod worth is an important neutronics parameter that plays a decisive role in the safe operation of a nuclear reactor. TRIGA

* *Corresponding author.*
E-mail address: drsiraj@comsats.edu.pk (S.-u.-I. Ahmad).

https://doi.org/10.1016/j.net.2017.11.003

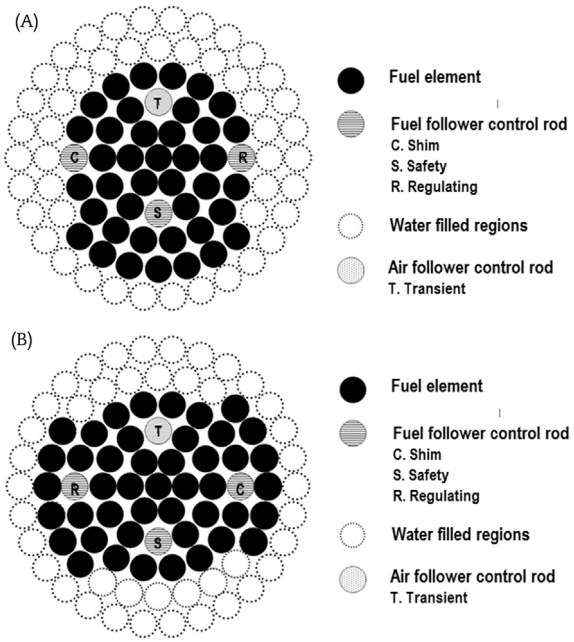

Fig. 1. Benchmark cores. (A) Core 133 is shown. (B) Core 134 is shown.

Table 1
Fuel element data [18].

Component	Dimension (cm)	Material	Density (g/cm^3)	Mass (g)
Fuel element outer radius	1.87706			
Fuel element length	72.06			
Fuel material		**U-ZrH**	**6.12**	
Fuel meat outer radius	1.82245			
Fuel meat inner radius	0.3175			
Fuel meat height	38.1			
Total fuel loading				2360
Average amount of U in each fuel element				277.9073
Average amount of U-235 in each fuel element				55.3035
Zr rod		**Zr**	**6.49**	
Zr rod inner radius	0.3175			
Zr rod height	38.1			
Cladding		**SS-304**	**7.88**	
Thickness	0.0508			

Mark II reactor core 134 has slightly more excess reactivity than core 133, as discussed earlier, and hence this core is chosen for the analysis of CR worth. Different procedures were used for modeling of CRs; the results are compared with experimental and Monte Carlo simulation results.

2. Materials and methods

2.1. TRIGA core configuration

The configurations of TRIGA benchmark cores 133 and 134 can be seen in Fig. 1. Core 133 is a symmetric core with 40 fuel elements containing three fuel follower CRs and one air follower CR, whereas core 134 has inverted symmetry, with 45 fuel elements having three fuel follower CRs and one air follower CR. Fuel elements of both the cores are of standard ST-12 type and contain U-ZrH as fuel with 19.9% enriched uranium. The details are given in Table 1. Fuel follower CRs have boron carbide in their upper portion followed by U-ZrH fuel. Each fuel follower CR has its special purpose and is used for safety, regulation, and shimming in TRIGA reactors. Similarly, the air follower CR (transient rod) has a neutron absorber portion, which is followed by air [18]. Geometric details of the fuel and air follower CRs are given in Table 2. The fuel loading and amount of U-235 are different in each fuel element and fuel follower CR. Therefore, average amount of fuel and amount of U-235 were calculated from the shipment data [18].

Table 2
Control rod data [18].

Component	Dimension (cm)	Material	Density (g/cm^3)	Mass (g)
Fuel Follower control rod				
Outer radius	1.74625			
Element length	111.125			
Fuel material		**U-ZrH**	**6.12**	
Outer radius	1.66495			
Inner diameter	0.3175			
Height	38.1			
Total fuel loading				1957.55
Average amount of U in each fuel follower control rod				235.6633
Average amount of U-235 in each fuel element				46.8933
Zr rod		**Zr**	**6.49**	
Radius	0.3175			
Absorber		**B_4C**	**2.10**	
Radius	1.66495			
Length	38.1			
Cladding		**SS-304**	**7.88**	
Thickness	0.0508			
Air follower control rod				
Outer radius	1.5875			
Element length	111.125			
Air follower		**Air**	**0.00123**	
Radius	1.525			
Height	55.25			
Absorber		**B_4C**	**2.10**	
Radius	1.525			
Length	38.1			
Cladding		**Aluminum**	**2.70**	
Thickness	0.0711			
Transient-rod guide tube		**Aluminum**	**2.70**	
Outer radius	1.9			

2.2. Computer codes

The computer codes used for criticality calculations include WIMSD and PRIDE. A brief overview of both codes is outlined below.

2.2.1. Winfrith Improved Multi-group Scheme-D

"Winfrith Improved Multi-group Scheme-D" [9] is a general-purpose lattice cell code based on the one-dimensional energy-dependent transport equation. It generates effective group constants such as diffusion coefficient (D), macroscopic absorption cross section (Σ_a), production cross section ($\nu\Sigma_f$), scattering matrix, etc., for use by diffusion codes for reactor analysis.

2.2.2. Program for Reactor In-core Analysis using Diffusion Equation

"Program for Reactor In-core analysis using Diffusion Equation" was developed by Ahmad et al. [1] to solve multigroup, multidimensional criticality problems. It can treat 1-, 2-, and 3-D slab geometries, 1-, 2-, and 3-D cylindrical geometries, and 1-D spherical geometry. The code is written in C language with dynamic memory allocation, with no internal restriction to number of regions, meshes, etc. A flux or multiplication gradient–based

Table 3
Sixty angular regions for both cores 133 and 134.

Region no.	Angle (degrees)	Region no.	Angle (degrees)	Region no.	Angle (degrees)
1	7.5	21	127.5	41	247.5
2	10	22	130	42	250
3	15	23	135	43	255
4	22.5	24	142.5	44	262.5
5	30	25	150	45	270
6	37.5	26	157.5	46	277.5
7	45	27	165	47	285
8	50	28	170	48	290
9	52.5	29	172.5	49	292.5
10	60	30	180	50	300
11	67.5	31	187.5	51	307.5
12	70	32	190	52	310
13	75	33	195	53	315
14	82.5	34	202.5	54	322.5
15	90	35	210	55	330
16	97.5	36	217.5	56	337.5
17	105	37	225	57	345
18	110	38	230	58	350
19	112.5	39	232.5	59	352.5
20	120	40	240	60	360

Table 4
Radial regions along with their radii for the both cores 133 and 134.

Region no.	Radius (cm)
1	2.0270
2	6.0175
3	9.9595
4	13.927
5	17.902
6	22.06
7	54.50
8	154.50

acceleration procedure is used. Mesh-centered central difference formulation has been programmed. The PRIDE has previously been validated for the light water reactor 3-D IAEA benchmark, designed for validations of course mesh methods [15]. Moreover, the PWR (Pressurized Water Reactors) experimental benchmark developed on the basis of experiments done in 1971 at Babcock and Wilcox's Lynchburg Research Center [5] was also analyzed with the code. The detailed results from PRIDE can be seen in articles by Ahmad and Sahibzada [3] and Arshad and Ahmad [6].

2.2.3. Modeling of the core in 2-D

To perform the simulations, the core was divided into 60 angular regions and eight radial regions. The first six radial regions are the active core regions, whereas region 7 represents the graphite reflector region. The outer region, i.e., region 8, represents the water surrounding the core. Table 3 shows the angular regions and corresponding starting angles (in degrees) with horizontal lines; Table 4 gives the radial regions and the corresponding radii. The angular regions were selected in such a manner that all the possible geometry changes in the core can be covered without changing the region dimensions. The model used for core 133, showing the angular and radial regions, is shown in Fig. 2. A similar model was developed for core 134. WIMSD was used for the generation of homogenized data for various regions. The details of these regions and the procedure used for homogenization are given in coming sections.

2.2.4. Analysis

The homogenized regions were modeled using various options in WIMSD to calculate the corresponding group constants to be

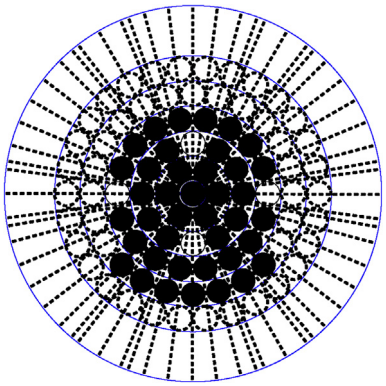

Fig. 2. The radial and angular regions for core 133.

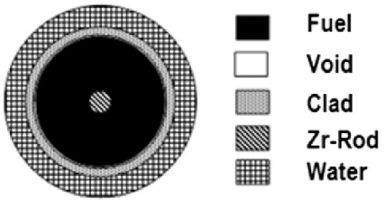

Fig. 3. Pin cell model of fuel element.

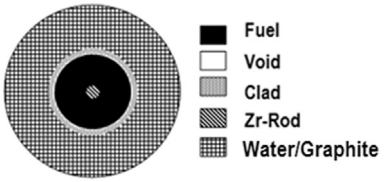

Fig. 4. Pin cell model for water-filled region or graphite reflector region.

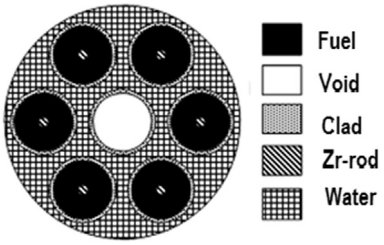

Fig. 5. Cluster model for the air/void region.

used in PRIDE. Regions defined for homogenization include fuel region of fuel elements, fuel region of fuel follower CRs, air/void region, water region, and graphite reflector region. Group constants for the fuel region of fuel elements and fuel follower CRs are calculated separately because there is a slight difference in the fuel material diameters, as shown in Tables 1 and 2. The pin cell model option of WIMS-D/4 is used for the fuel, water, and graphite reflector regions, whereas for the air region, the cluster option is used. The fuel element pin cell model comprising the fuel element and the surrounding water region is shown in Fig. 3. For the generation of group constants for the water and graphite reflector regions, a large water or graphite region surrounding the fuel cell is modeled as given in Fig. 4. The REGION card option of WIMS-D/4 is used to extract the group constants of the required region. For the generation of group constants for the air and surrounding fuel elements, the cluster option of WIMSD was used, comprising an air

region followed by clad and a guide tube made of aluminum surrounded by fuel elements. Fig. 5 shows the cluster model for air/void regions.

The lattice cell calculations are performed for four condensed energy groups with the upper and lower energy boundaries given in Table 5. The weight fractions for materials in different WIMSD regions are given in Table 6. The same group constant generation procedure was repeated for all five cross-section libraries.

The axial buckling value was 0.0052 cm^{-2}. The group constants were generated from WIMS-D/4 for each region of the core and were input to PRIDE for whole core calculations. All the core calculations were performed using convergence criteria of 10^{-6} as relative difference in flux in two successive iterations.

2.2.5. Results of 2-D modeling

The calculated effective multiplication factors for core 133, along with the experimental results, are given in the Table 7. In addition, the Monte Carlo results reported with Monte Carlo N-Particle Transport Code (MCNP) code [24] are also included. In Table 8, the simulation results for core 134 are given along with the experimental results and results obtained with the MCNP code. It can be seen from both tables that the simulation results are in good agreement with the experimental results, and with the Monte Carlo code results, within 1%. In both cases among all libraries, ENDF/B-VI.8 gives the lowest value of multiplication factor, and the JEF-2.2 library gives the maximum value. In case of core 133, the nearest match with the experimental value is for the JEF-2.2 library, with a deviation of 0.13%, whereas ENDF/B-VI.8 gives the maximum deviation, i.e., 0.82%. In the case of core 134, the IAEA library results are closest to the experimental results, with a deviation of 0.05% whereas, in this case, ENDF/B-VI.8 again gives the maximum deviation, i.e., 0.46%, in the results.

2.3. Modeling of core in 3-D

All the regions in the axial direction of the cores have to be considered in this case. For simplicity, the molybdenum plates in the active core region and grid plates have not been included in the analysis. The radial and angular regions of the core were the same as used in the 2-D calculations. However, in the axial direction, 13 regions are considered for the six major sections of the core, as discussed previously. A total length of ~139 cm in the axial direction is modeled by dividing it into various axial sections depending on the composition of the materials. The major sections of the core are fuel, fuel follower CR, transient CR, water in the core, radial and axial graphite reflectors, and water reflector, with their axial variations as shown in Fig. 6.

2.3.1. Simulation procedure

For 3-D analysis, group constants for the stainless steel, axial graphite, void, and boron carbide are also required. All the group constants are calculated using pin cell or cluster options of WIMS-D/4. Boron carbide cross sections are used for CR worth calculations using the same 3-D model. Calculations were carried out with 14 energy groups. The details of the group boundaries are given in Table 9. The generated group constants are used along with the 3-D core model to calculate the multiplication factor. The convergence criterion was set at 10^{-6} according to the tolerance in flux in consecutive iterations.

Table 5
Energy boundaries for the condensed energy groups.

Group no.	Group of library	Upper energy boundary (eV)	Lower energy boundary (eV)
1	1–16	1.000×10^{7}	5.530×10^{3}
2	16–26	5.530×10^{3}	1.596×10^{1}
3	26–46	1.596×10^{1}	6.250×10^{-1}
4	46–69	6.250×10^{-1}	5.000×10^{-3}

Table 6
Calculated weight fraction of various isotopes used for the generation of group constants.

Material	Isotope	Weight %
Fuel material in fuel element (U-ZrH)	U-238	9.4309
	U-235	2.3427
	Zr-nat	86.6566
	H-1	1.5698
Fuel material in fuel follower control rod (U-ZrH)	U-238	9.643
	U-235	2.396
	Zr-nat	86.394
	H-1	1.567
Coolant material (light water)	H-1	11.19
	O-16	88.81
Reflector material (graphite)	C-12	100.0
Cladding material for fuel element and fuel follower control rod (SS-304)	Fe-nat	69.5183
	Cr-nat	19.0086
	Ni-nat	9.38436
	Mn-nat	2.08874
Cladding material for air follower control rod (aluminum)	Al-nat	100.0
Boron carbide for fuel follower control rod	B-10	13.69
	B-11	64.59
	C-12	21.72

Table 7
2-D modeling results of core 133.

Code	Library	Multiplication factor	Percentage difference with experimental value (%)
PRIDE	IAEA	0.99871	0.40
	ENDF/B-VII.0	1.00014	0.26
	JEFF-3.1	0.99632	0.64
	ENDF/B-VI.8	0.99451	0.82
	JENDL-3.2	0.99869	0.40
	JEF-2.2	1.00146	0.13
MCNP (Z agar et al., [24])		1.00629	0.35
Experimental (Z agar et al., [24])		1.00277	—

Table 8
2-D modeling results of core 134.

Code	Library	Multiplication factor	Percentage difference with experimental value (%)
PRIDE	IAEA	1.01962	0.05
	ENDF/B-VII.0	1.02103	0.08
	JEFF-3.1	1.01732	0.28
	ENDF/B-VI.8	1.01547	0.46
	JENDL-3.2	1.01952	0.06
	JEF-2.2	1.02239	0.21
MCNP (Z agar et al., [24])		1.02386	0.36
Experimental (Z agar et al., [24])		1.02020	—

2.3.2. Results of 3-D modeling

3-D results of both the cores are given in Tables 10 and 11. The results are compared with reference experimental values, and differences in reactivity values are also calculated. It can be seen that the 3-D results are in good agreement with the experimental results because percentage error for both cases (i.e., core 133 and core 134) is less than 1%. The difference in calculated and measured data is due to various reasons including simplified modeling approximations in diffusion calculations and uncertainties in measured

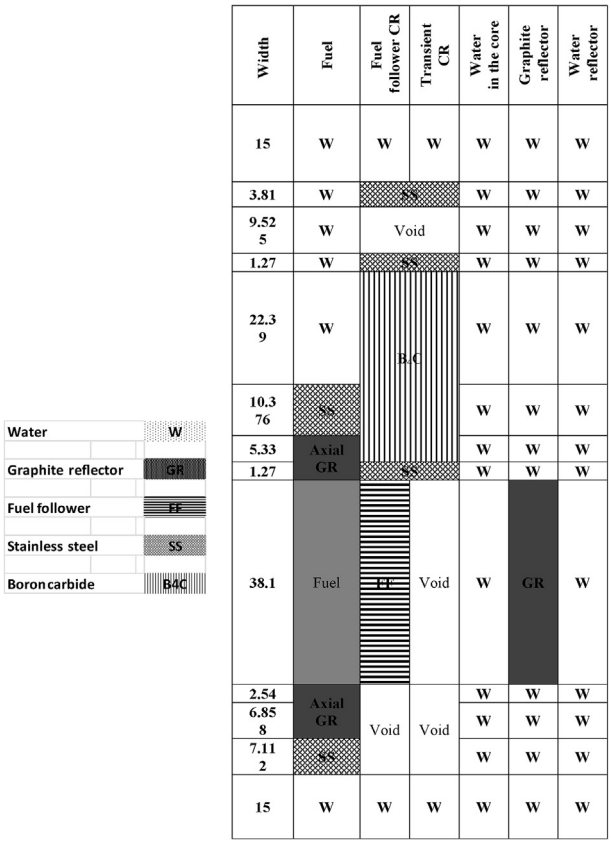

Fig. 6. Axial regions used for 3-D modeling of core 133 and core 134.

values. According to shipment data, uncertainties in U-235 values results in 60 pcm uncertainty in the multiplication factor. The other uncertainties are uncertainty in the uranium concentration in the U-ZrH mixture and uncertainties in the H/Zr ratio. The total fuel material composition uncertainty is reported to be around 250 pcm [11].

2.3.3. CR worth calculations

Owing to the availability of experimental results, as well as results from Monte Carlo simulations, core 134 was used for the calculation of the CR worth. The rod insertion method was used in the analysis, with two different homogenization models: one based on less homogenization of the CR, i.e., only the CR region, whereas the other was based on homogenization of the CR and the surrounding fuel rods in a single region. A CR surrounded by six neighboring fuel elements is modeled in WIMS-D/4 using its cluster option, similar to the cluster presented in Fig. 5 for voids. The results for multiplication factor in the 3-D clean core calculations show that for core 134, the ENDF/B-VI.8 library resulted in the nearest match with the experimental data. Moreover, the ENDF/B-V cross-section data have been used in the Monte Carlo simulations; therefore, we have used the ENDF/B-VI.8 data–based WIMSD library in our simulations for CR worth. Where needed, the group constants for CRs are extracted using the REGION card in WIMSD input. For 3-D modeling in PRIDE, Fig. 6 is used, in which the active core region of 38.1 cm is divided into eight regions (7 regions of 5 cm and 1 region of 3.1 cm) for reactivity worth calculation.

Table 9
Energy boundaries for the condensed energy groups.

Group no.	Group of library	Upper energy boundary (eV)	Lower energy boundary (eV)
1	1–5	1.000×10^{7}	1.353×10^{6}
2	5–10	1.353×10^{6}	1.110×10^{5}
3	10–15	1.110×10^{5}	9.118×10^{3}
4	15–20	9.118×10^{3}	9.068×10^{2}
5	20–25	9.068×10^{2}	2.770×10^{1}
6	25–30	2.770×10^{1}	2.600×10^{0}
7	30–35	2.600×10^{0}	1.123×10^{0}
8	35–40	1.123×10^{0}	9.960×10^{-1}
9	40–45	9.960×10^{-1}	7.800×10^{-1}
10	45–50	7.800×10^{-1}	3.200×10^{-1}
11	50–55	3.200×10^{-1}	1.800×10^{-1}
12	55–60	1.800×10^{-1}	5.800×10^{-2}
13	60–65	5.800×10^{-2}	2.500×10^{-2}
14	65–69	2.500×10^{-2}	5.000×10^{-3}

Table 10
3-D modeling results of core 133.

Code	Library	Multiplication factor	Percentage difference with experimental results (%)
PRIDE	IAEA	1.00131	0.14
	ENDF/B-VII.0	1.00132	0.14
	JEFF-3.1	0.99875	0.40
	ENDF/B-VI.8	0.99673	0.60
	JENDL-3.2	1.00059	0.21
	JEF-2.2	1.00424	0.14
MCNP (Z agar et al., [24])		1.00629	0.35
Experimental (Z agar et al., [24])		1.00277	—

Table 11
3-D modeling results of core 134.

Code	Library	Multiplication factor	Percentage differences with experimental results (%)
PRIDE	IAEA	1.02518	0.48
	ENDF/B-VII.0	1.02518	0.48
	JEFF-3.1	1.02245	0.22
	ENDF/B-VI.8	1.02057	0.03
	JENDL-3.2	1.02434	0.40
	JEF-2.2	1.02796	0.76
MCNP (Z agar et al., [24])		1.02386	0.36
Experimental (Z agar et al., [24])		1.02020	—

First of all, excess reactivity worth is calculated by considering all the CRs out of the core. For the calculation of the worth of each individual CR, the following method is used.

I. One of the CRs was selected. (e.g., Shim CR)
II. Insertion length was taken as $z = 5$ cm.
III. Group constants for the selected rod are used for z cm from the top of the core, keeping all other CRs at out position (no change in group constants at these positions).
IV. The effective multiplication factor was calculated.
V. The worth of CR was calculated using the following relation

$$\rho(z) = \frac{1}{k_{out}} - \frac{1}{k_{in}(z)}$$

where k_{out} is the multiplication factor of clean core and $k_{in}(z)$ is the multiplication factor of the core with one rod inserted to $z$cm.

VI. Insertion length of the CR was increased to 10, 15, 20, 25, 30, 35, and 38.1 cm, and steps III and V were repeated.
VII. Steps II–VI were repeated for safety CR, transient CR, and regulating CR.

CR worth results using WIMS-D/4 and PRIDE are shown in Tables 12–15 and Figs. 7–10. Results are compared with the experimental results and the Monte Carlo simulation results

Table 12
Reactivity worth of shim control rod.

Insertion (cm)	Experimental (pcm)	Reactivity (pcm)		Absolute deviation (%)	
		PRIDE	KenoV.a (±70)	PRIDE	KenoV.a
5	71	231	260	225	266
10	305	637	376	109	23
15	686	1202	902	75	31
20	1160	1844	1344	59	16
25	1619	2443	1760	51	9
30	1997	2869	2110	44	6
35	2232	3083	2341	38	5
38.1	2290	3170	2311	38	1

Table 13
Reactivity worth of safety control rod.

Insertion (cm)	Experimental (pcm)	Reactivity (pcm)		Absolute deviation (%)	
		PRIDE	KenoV.a (±70)	PRIDE	KenoV.a
5	83	316	192	281	131
10	369	883	716	139	94
15	873	1697	1265	94	45
20	1562	2670	2100	71	34
25	2328	3622	2898	56	24
30	3003	4335	3431	44	14
35	3453	4699	3637	36	5
38.1	3592	4788	3606	33	0

Table 14
Reactivity worth of transient control rod.

Insertion (cm)	Experimental (pcm)	Reactivity (pcm)		Deviation (%)	
		PRIDE	KenoV.a (±70)	PRIDE	KenoV.a
5	90	375	154	317	71
10	302	994	512	229	70
15	667	1863	970	179	45
20	1149	2888	1423	151	24
25	1667	3883	1920	133	15
30	2103	4626	2261	120	8
35	2400	5014	2392	109	0
38.1	2476	5012	2493	102	1

Table 15
Reactivity worth of regulating control rod.

Insertion (cm)	Experimental (pcm)	Reactivity (pcm)		Deviation (%)	
		PRIDE	KenoV.a (±70)	PRIDE	KenoV.a
5	70	233	67	233	4
10	312	639	405	105	30
15	742	1209	892	63	20
20	1347	1853	1393	38	3
25	2040	2451	1790	20	12
30	2684	2880	2211	7	18
35	3110	3095	2372	0	24
38.1	3227	3148	2331	2	28

obtained by KenoV.a code using rod insertion method [23]. For all CRs, the diffusion calculation overestimates the CR worth. The deviation in rod worth increases with an increase in the insertion depth; however, the percent deviation decreases with an increase in the insertion depth due to the increase in worth. Table 12 presents the reactivity worth of the shim CR. The percent deviation is large for 5 cm insertion in both Monte Carlo and diffusion calculations and decreases with an increase in the insertion length. The deviation in worth calculated by KenoV.a is within the uncertainty in the calculations (i.e., 70 pcm), whereas PRIDE results have minimum deviation of 38% in case of full insertion. Similar behavior is seen for the safety CR. The trends of percent deviation in the case

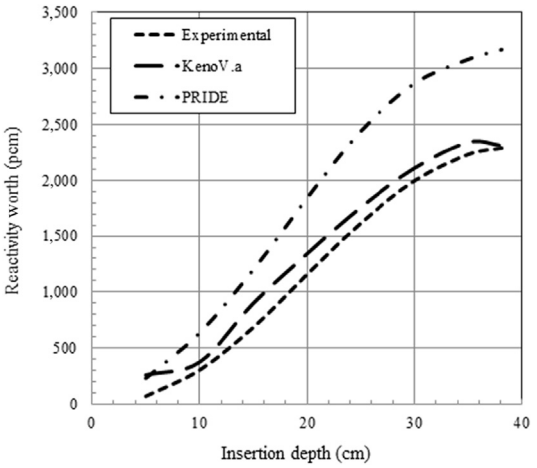

Fig. 7. Shim control rod worth.

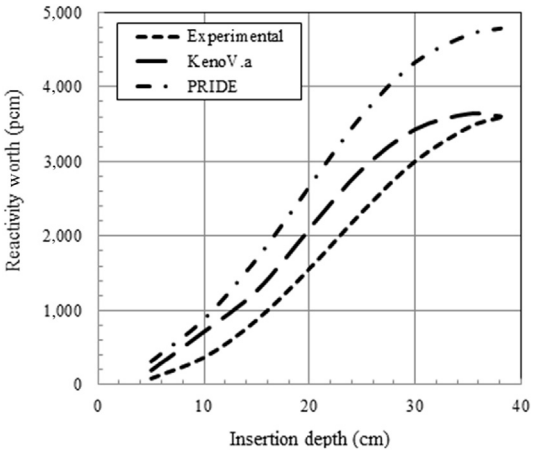

Fig. 8. Safety control rod worth.

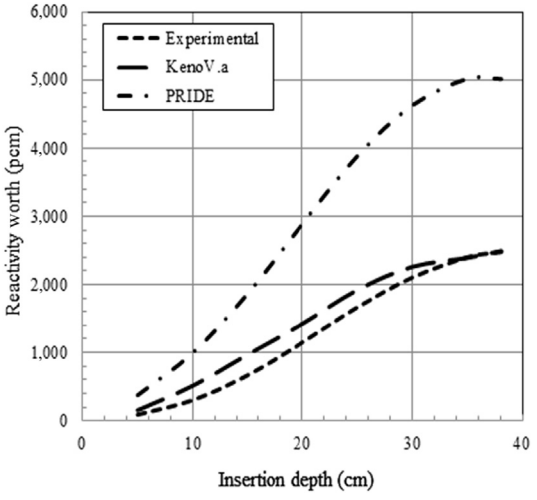

Fig. 9. Transient control rod worth.

of PRIDE and KenoV.a vary in a manner similar to that of the shim CR, with a minimum deviation of 33% in the case of PRIDE and less than 1% in the case of KenoV.a. In the case of the transient CR, there are maximum deviations in worth from PRIDE, with a minimum value of 102% at full insertion. The experimental values in the case

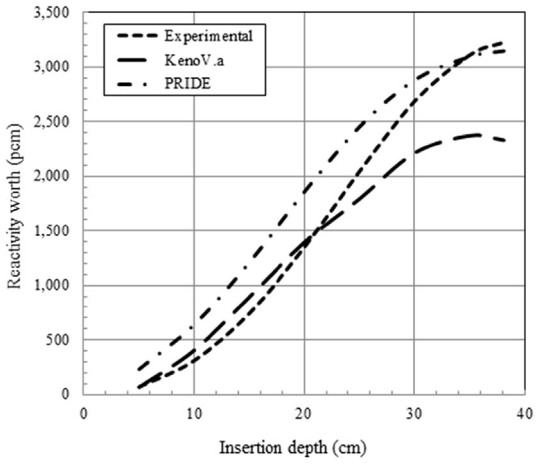

Fig. 10. Regulating control rod worth.

Table 16
Reactivity worth of shim control rod.

Insertion (cm)	Experimental (pcm)	Reactivity (pcm)		Absolute deviation (%)	
		PRIDE	KenoV.a (±70)	PRIDE	KenoV.a (±70)
5	71	103	260	45	266
10	305	342	376	12	23
15	686	693	902	1	31
20	1160	1108	1344	4	16
25	1619	1509	1760	7	9
30	1997	1818	2110	9	6
35	2232	1992	2341	11	5
38.1	2290	2038	2311	11	1

Table 17
Reactivity worth of safety control rod.

Insertion (cm)	Experimental (pcm)	Reactivity (pcm)		Absolute deviation (%)	
		PRIDE	KenoV.a (±70)	PRIDE	KenoV.a (±70)
5	83	153	192	84	131
10	369	521	716	41	94
15	873	1071	1265	23	45
20	1562	1743	2100	12	34
25	2328	2422	2898	4	24
30	3003	2960	3431	1	14
35	3453	3266	3637	5	5
38.1	3592	3341	3606	7	0

Table 18
Reactivity worth of transient control rod.

Insertion (cm)	Experimental (pcm)	Reactivity (pcm)		Absolute deviation (%)	
		PRIDE	KenoV.a (±70)	PRIDE	KenoV.a (±70)
5	90	91	154	1	71
10	302	339	512	12	70
15	667	722	970	8	45
20	1149	1188	1423	3	24
25	1667	1647	1920	1	15
30	2103	2005	2261	5	8
35	2400	2195	2392	9	0
38.1	2476	2244	2493	9	1

of regulating the CR are not reliable because there was some error introduced during the experiment [19]. This is also reflected in the KenoV.a results, in which the experimental values in most cases deviate more than the uncertainty in the simulation results.

Table 19
Reactivity worth of regulating control rod.

Insertion (cm)	Experimental (pcm)	Reactivity (pcm)		Absolute deviation (%)	
		PRIDE	KenoV.a (±70)	PRIDE	KenoV.a (±70)
5	70	103	67	147	96
10	312	343	405	110	130
15	742	674	892	91	120
20	1347	1112	1393	83	103
25	2040	1516	1790	74	88
30	2684	1828	2211	68	82
35	3110	2007	2372	65	76
38.1	3227	2047	2331	63	72

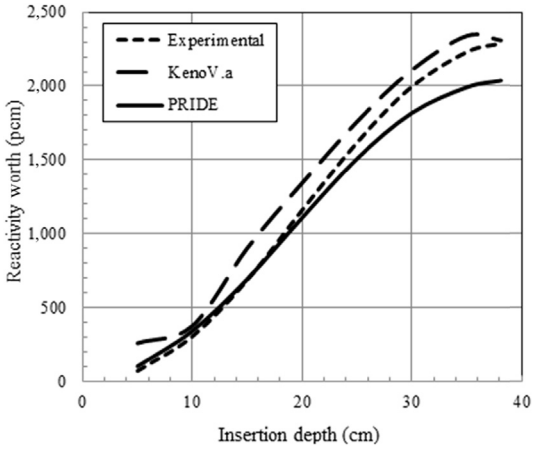

Fig. 11. Shim control rod worth.

It can also be seen in the tables that the reported KenoV.a value for CR worth for 38.1 cm is less than that for 35 cm; however, the difference is less than the uncertainty in the calculation. This is probably indicative of nonaccurate modeling in KenoV.a for full insertion positions.

2.4. Improved model for CR worth calculations

In this model, the group constants for a whole cluster calculated, from WIMS-D/4, are given as input to the PRIDE code. Therefore, instead of using group constants of a single CR, homogenized group constants of the CRs and the adjacent fuel elements are calculated and given as input. However, the rest of the procedure for the calculation of CR worth is similar to the less homogenization model.

The results are given in Tables 16–19 and Figs. 11–14. It can be seen that, in this case, the diffusion theory code gives better results, with reduced deviations. In the case of the shim CR, the deviation dropped to 1–45% compared with the previous case, where it was 38–225%. For the safety CRs, the deviation dropped to a maximum of 1–84% as compared with 33–281%. The deviations for the transient rod also dropped from 102–317% to 1–12%, whereas for the regulating CR, the deviations from the experimental data did not significantly drop. The deviations for regulating CR are also large in the case of KenoV.a. However, compared with the previous modeling, there is a significant decrease in the difference between the PRIDE results and the KenoV.a results. The experimental data for this case are not reliable due to the high uncertainty, as reported by Mele et al. [18]. This was due to the close positioning of the detector and the regulating rod, which resulted in local flux perturbations and increased uncertainties in the measured values.

It can be observed that, compared with the procedure given in the previous section, except for the regulating CR, the results from this procedure are close to the experimental results, whereas in

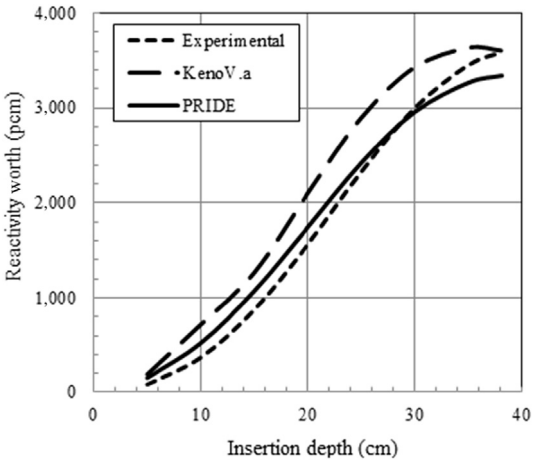

Fig. 12. Safety control rod worth.

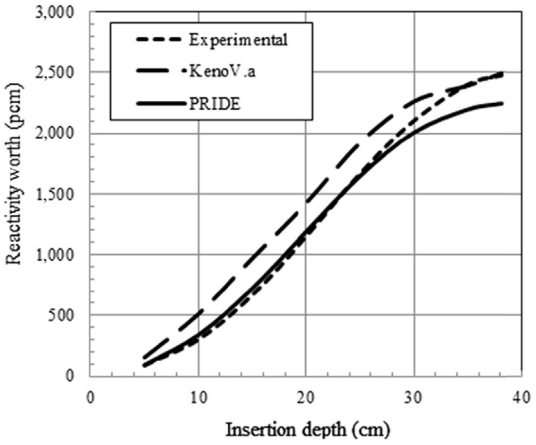

Fig. 13. Transient control rod worth.

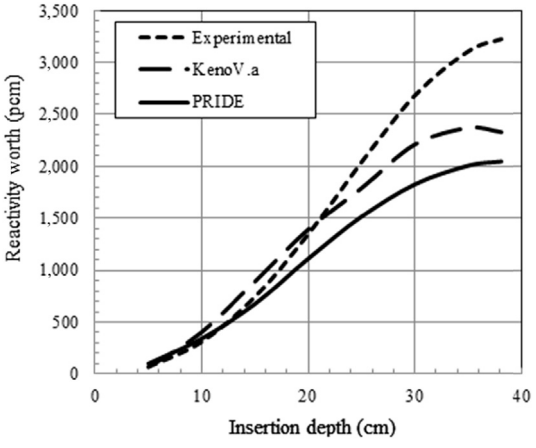

Fig. 14. Regulating control rod worth.

the case of the regulating CR, the results became closer to the reported Monte Carlo simulation results. When extracted CR group constants were used separately, i.e., in the previous case, the large deviations are attributed to sharp variation in the neutron flux from the fuel element region to the boron carbide region. However, in the present case, there is a gradual change in the neutron flux due to the homogenization of the CR and the surrounding fuel elements region. Hence, this calculation methodology gives results that are in good agreement with both the experimental results and the reported results of Monte Carlo calculations based on code KenoV.a.

3. Conclusions

Using WIMSD and PRIDE codes for 2-D and 3-D core models, TRIGA Mark-II benchmark cores 133 and 134 were analyzed for clean core reactivity. Moreover, the CR worth values for core 134 were calculated by rod insertion method, and results were compared with Monte Carlo and experimental results. Different WIMSD cross-section libraries including ENDF/B-VI.8, ENDF/B-VII.0, JENDL-3.2, JEF-2.2, and JEF-3.1 were used for homogenized group constant generation. It was found that the clean core multiplication factor using 2-D or 3-D model is in good agreement with reported values. For the calculation of CR worth, taking only the absorber region separately in the diffusion code without homogenization at cell level with surrounding fuel rods led to larger deviation in CR worth values. However, using proper homogenization of the CRs and surrounding regions for group constant dr4 generation, the calculated values of CR worth significantly improved.

Conflict of interest

The authors declare that, there is no conflict of interest.

References

[1] Ahmad, S. I. and Gul, R., PRIDE v-3.1, 2012, A multidimensional multigroup reactor analysis code, user manual, reactor analysis group, Pakistan Atomic Energy Commission.
[2] S.I. Ahmad, N. Ahmad, Aslam, Effect of new cross-sections evaluation on criticality and neutron energy spectrum of a typical material test research reactor, Ann. Nucl. Energy 31 (2004) 1867–1881.
[3] S.I. Ahmad, T.M. Sahibzada, Moderator temperature effects on reactivity of HEU core of MNSR, Ann. Nucl. Energy 49 (2012) 207–211.
[4] D.L. Aldama, F. Leszczynski, A. Trokov, IAEA Coordinated Research Project, WIMS-D library update Project, IAEA, Vienna, 2003.
[5] ANS, "PWR lattice benchmark problems", Ad Hoc Committee on reactor physics benchmarks, reactor physics division mathematics & Computation division, Am. Nucl. Soc. (1996). April 1996.
[6] F. Arshad, S.I. Ahmad, PWR experimental benchmark analysis using WIMSD and PRIDE codes, Ann. Nucl. Energy 72 (2014) 11–19.
[8] Chadwick, et al., ENDF/B-VII.0: Next generation evaluated nuclear data library for nuclear science and technology, Nucl. Data Sheets 107 (2006) 2931–3060.
[9] M.J. Halsall, A Summary of WIMS-D/4 Input Options, AEE, Winfrith, 1980.
[11] R. Jeraj, A. Peršič, T. Zagar, M. Ravnik, Sensitivity studies of TRIGA benchmark critical experiment, nuclear energy in central Europe '99, portorož, Slovenia, 1999, 6 to 9 September, 1999.
[13] A. Koning, et al., The JEFF-3.1 nuclear data library, nuclear energy agency, NEA, 2006, p. 6190.
[15] R.R. Lee, et al., Multidimensional (x-y-z) LWR Model., ANL-7416 Supplement 2, Argonne National Laboratory, 9700 South Avenue, Argonne, Illinois 60439, 1977.
[16] H.D. Lemmel, P.K. McLaughlin, V.G. Pronyaev, The U.S. Evaluated Nuclear Data Library for Neutron Reaction Data by the US National Nuclear Data Center, Nuclear data section, International Atomic Energy Agency, ENDF/B-VI release 8 (Last release of ENDF/B-VI), 2001. IAEA-NDS-100 Rev. 11, Nov. 2001.
[18] I. Mele, M. Ravnik, A. Trokov, TRIGA Mark II benchmark experiment, Part I: steady state operation, Nucl. Technol. 105 (1994a) 37–51.
[19] I. Mele, M. Ravnik, A. Trkov, TRIGA Mark II benchmark experiment, Part II: pulse operation, Nucl. Technol. 105 (1994b) 52–58.
[20] T. Nakagawa, et al., Japanese evaluated nuclear data library, version 3 revision-2; JENDL-3.2, J.Nucl. Sci. Technol. 32 (1995) 1259–1271.
[22] M. Ravnik, Description of TRIGA Reactors, Joseph Stefan's Institute, Ljubljana, Slovenia, 2012. Retrieved from: http://www.rcp.ijs.si/ric/description-s.html.
[23] M. Tombakoglu, Y. Çeçen, Control rod worth evaluation of TRIGA Mark II reactor, in: International Conference, Nuclear Energy in Central Europe, Hoteli Bernardin, Portorož, Slovenia, 10 to 13 September, 2001, 2001.
[24] T. Zagar, A. Persic, R. Jeraj, M. Ravnik, Simulation of the TRIGA Mark II benchmark experiment with burned fuel, in: International Conference, Nuclear Energy in Central Europe' 99, Portorož, Slovenia, 6 to 9 September, 1999, 1999.